Electronic Structure of Carbon Nanotubes with Ultrahigh Curvature

Wolfgang Plank,[†] Rudolf Pfeiffer,[†] Christoph Schaman,[†] Hans Kuzmany,*[,†] Matteo Calvaresi,[‡] Francesco Zerbetto,[‡] and Jannik Meyer[§]

[†]Faculty of Physics, University of Vienna, Strudlhofgasse 4, A-1090 Wien, Austria, [‡]Institute of Inorganic Chemistry, University of Bologna, 40126 Bologna, Italy, and [§]University of Ulm, Albert Einstein Allee 11, D-89081 Ulm, Germany

ABSTRACT The electronic and the vibrational structure of carbon nanotubes with ultrahigh curvature was systematically studied by resonance Raman scattering, high-resolution transmission electron microscopy (HRTEM), molecular dynamics, and *ab initio* DFT calculations. The ultrahigh curvature tubes were grown inside commercial HiPco tubes after filling the latter with the small but carbon-rich molecule ferrocene. TEM showed partial filling of the outer tubes with inner tubes and mobility of the latter in the electron beam. The smallest analyzed tube was of (5,0) chirality and had a DFT determined diameter of 0.406 nm and a radial breathing mode frequency of 570 cm^{-1}. For all inner tubes which had transitions in the visible spectral range, transition energies and RBM frequencies were determined with a resonance width of only 45 meV. Experimentally determined transition energies revealed dramatic deviations up to several electronvolts compared to tight-binding calculations and a significant family spread of more than 2 eV but were in agreement with many electron contribution corrected extended tight-binding results and with results from DFT calculations.

KEYWORDS: ultrahigh curvature carbon nanotubes · electronic structure · resonance Raman · electron correlation · atomic resolution TEM

Single-walled carbon nanotubes (SWCNTs) have been attracting considerable interest for a number of years as they are prototypes of one-dimensional systems on the one hand and exhibit a high application potential on the other hand.[1−3] The simplest way to obtain the electronic structure of the tubes is to evaluate it from graphene by transversal zone folding with a ribbon width corresponding to the circumference of the tubes. This works well until, with decreasing diameter, the increasing curvature of the tubes requires the consideration of contributions from σ-bonded electrons and the curvature-induced anisotropy of the transfer integrals becomes important. The geometry of such very narrow tubes and their electronic ground state have been reported repeatedly from first-principle density functional theory (DFT) calculations,[4] even up to the GW level, and in few special cases, the effects of excitonic bonding were considered.[5,6] As the many electron effects increase the electron energy scale and excitons noticeably reduce transition energies, the two effects are known to more or less balance each other, which is considered the reason for the rather good agreement of experiments with simple or extended tight-binding calculations or with DFT calculations. However, a systematic study of response functions in this range of tube diameters is missing, even though the σ−π mixture introduces dramatic changes to the electronic structure,[7,8] is expected to enhance the electron−phonon[9−11] and spin−orbit coupling,[12] and eventually leads, under certain circumstances, to superconductivity.[13] One reason for the lack of the theoretical results is the lack of corresponding experiments. Even though single species of very narrow tubes, down to the 0.4 nm range, were grown in the channels of zeolite crystals,[14] the lack of a full set of extremely high curvature tubes prevented so far a check of the expected dramatic deviation of their electronic structure from the tight-binding results.

An alternative way to get access to the electronic structure of very high curvature tubes is to study the inner tubes of double-walled carbon nanotubes (DWCNTs). Such tubes are conveniently grown from annealing C_{60} peapods. However, rather high temperatures on the order of 1100 °C are required[15] since in this case transformation was shown to be established by fusion of C_{60} cages.[16] The diameter of the inner tubes is determined by the outer tube size reduced by twice the van der Waals distance, resulting in a 0.66 nm diameter reduction. However, due to the large size of the fullerenes in this way only tubes with diameters not smaller than 0.7 nm can be grown. Alternatively, growth of DWCNTs was also demonstrated from ferrocene ($FeCp_2$)

*Address correspondence to hans.kuzmany@univie.ac.at.

Received for review March 25, 2010 and accepted July 12, 2010.

Published online July 27, 2010. 10.1021/nn100615d

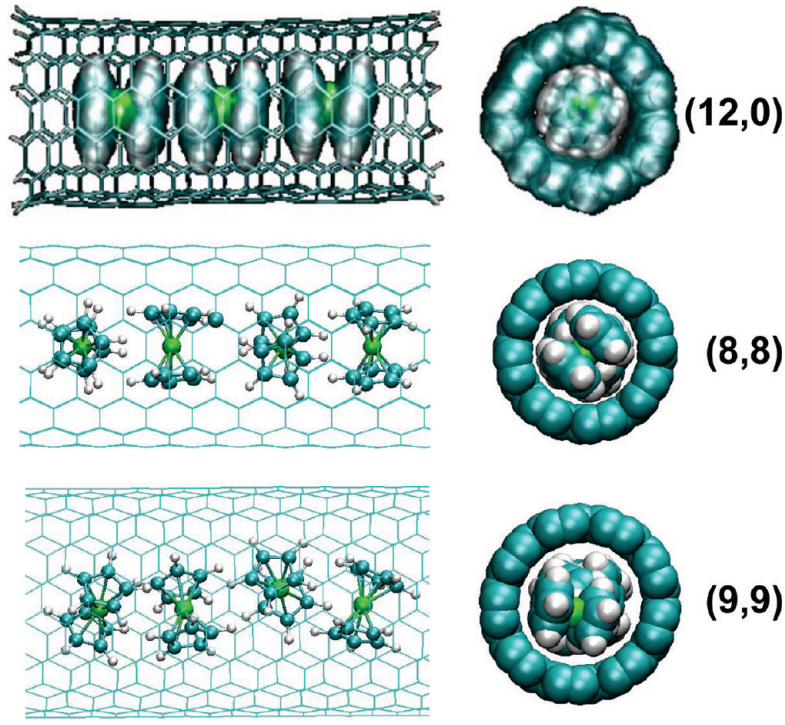

Figure 1. Calculated structures for $FeCp_2$@SWCNT. Top: $FeCp_2$@(12,0), d_t = 0.94 nm, binding energy = 1.19 eV per molecule, with van der Waals representation. Center: $FeCp_2$@(8,8), d_t = 1.09 nm, binding energy = 1.48 eV. Bottom: $FeCp_2$@(9,9), d_t = 1.22 nm, binding energy = 1.16 eV.

peapods.[17] Since ferrocene is considerably smaller than C_{60}, the growth of much thinner inner tubes can be expected. In addition, transformation temperatures of ferrocene to inner tubes are much lower and can go down to only 500 °C as discovered most recently.[18] The possibility to grow such very high curvature tubes from ferrocene was indeed demonstrated recently from a TEM study.[19]

Making use of the advantage of $FeCp_2$ as a filler, we demonstrate the existence of a full set of nanotubes with ultrahigh curvature by using a starting material with a diameter distribution centered at 1.1 nm. For the rather large subset of these tubes, which have optical transitions in the visible spectral range, we determine transition energies by resonance Raman scattering of the radial breathing mode and provide thus for the first time an extensive set of data related to electronic structure of the ultrahigh curvature tubes. Transmission electron microscopy confirmed the successful transformation of the $FeCp_2$ peapods to DWCNT and demonstrated that the inner tubes are mobile inside the nano cleanroom provided by the outer tubes. Experimental results are backed up by molecular dynamics calculations which revealed the binding energies of the incorporated ferrocene and the amount of carbon available for inner tube growth. Concerning the electronic structure, *ab initio* DFT calculation from the Siesta package and extended tight-binding calculations including many electron corrections provided very good agreement with the experiments and demonstrated explicitly the breakdown of family behavior for the tubes.

RESULTS AND DISCUSSION

The binding energies for the $FeCp_2$ molecule in the tubes were evaluated from extended molecular dynamical calculations (for details, see Supporting Information). Figure 1 depicts three examples of $FeCp_2$ peapod structures calculated for different tube diameters. The interaction between the tubes and the molecules determines a minimal diameter for exothermic encapsulation of 0.95 nm (tight binding diameter of the (12,0) NT) with binding energy of 1.19 eV per molecule. This diameter limit is in good agreement with the experi-

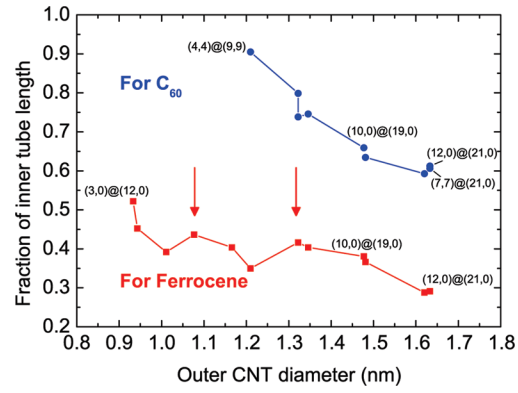

Figure 2. Fractional length of inner shell CNT for optimum filling with $FeCp_2$ (bottom curve) and with C_{60} (top curve). Arrows pointing toward the bottom curve indicate increased carbon availability for inner tube growth due to changes in the structural arrangement of $FeCp_2$.

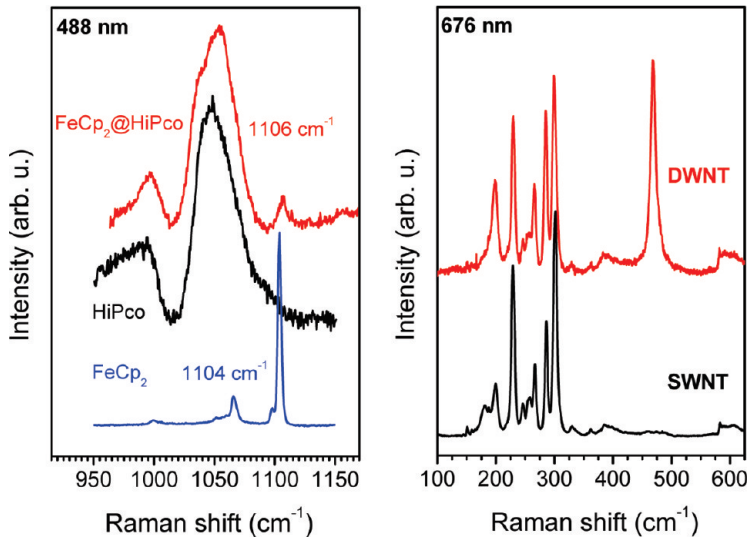

Figure 3. Raman spectra for $FeCp_2$ (bottom), for empty HiPco tubes in the intermediate frequency range (center), and $FeCp_2$@SWCNT (top) (left), and comparison between Raman spectra of $FeCp_2$ filled and transformed nanotubes (right).

mentally determined value for a comparable system analyzed by Nicholas and co-workers.[20] The highest binding energy of 1.49 eV was obtained for a (13,0) tube. In general, the observed binding energies were about a factor of 2 smaller compared to C_{60}@SWCNT. The top pattern in Figure 1 depicts the structure in a full van der Waals representation, which demonstrates the tight packing of the encapsulated molecule. With increasing tube diameter, the orientation of the ferrocene molecule changes from axially aligned to perpendicularly aligned, as depicted by the pattern for (8,8) and (9,9) in the figure. Eventually, for large diameter tubes, the $FeCp_2$ molecules staple in parallel arrangements and finally settle off axis.

Altogether, the filling conditions for 14 different tubes were investigated in the diameter range between 0.9 and 1.7 nm. From the results, it is possible to evaluate the total carbon resources which can be provided. In turn, by assuming a van der Waals distance of 0.33 nm between the concentric tubes, the total inner tube length can be calculated relative to the total length of the outer tubes. Results are depicted in Figure 2. Evidently, smaller diameter tubes give a better filling ratio of up to more than 50%, whereas conventional tubes with diameters in the range of 1.4 nm allow only for filling factors of less than 40%. The structures in the curve reflect the changes in geometrical arrangements of the encapsulated molecules in the peapod precursor. The figure also shows for comparison the results for C_{60} peapods. The trend for less good filling of the larger tubes is evident, and the limit for the possibility to fill small diameter tubes is also clearly seen. On the other hand, due to the high carbon concentration in C_{60}, filling up to 90% can be obtained. As it will be shown below, the findings for $FeCp_2$ are fully consistent with the experimental results.

Experimental data from the Raman spectra confirm the successful filling of the HiPco tubes, as depicted in Figure 3. The spectrum at the top clearly shows the response from the encapsulated molecules at 1106 cm^{-1}, even though the intensity of the line is rather weak, only about 10^{-4} from the G line of the tubes. The other lines observed in the spectrum are intermediate frequency modes of the tubes, which became clearly visible due to the strong blow up of the spectrum. The two spectra below were recorded from unfilled HiPco tubes and for polycrystalline $FeCp_2$ powder.

After transformation to DWCNTs, the response from $FeCp_2$ disappeares and new lines in the 350 to 600 cm^{-1}

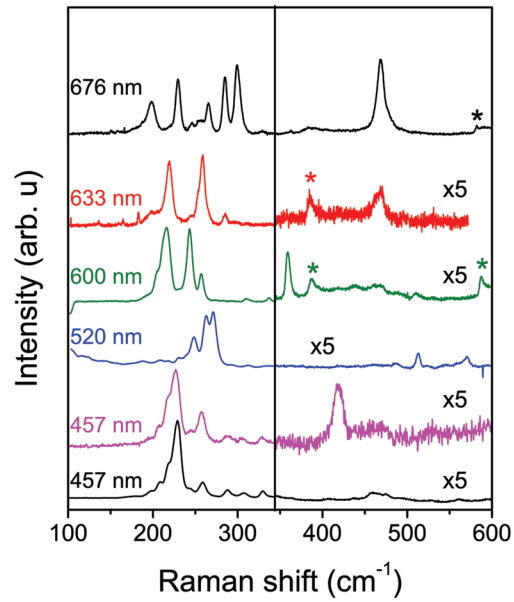

Figure 4. Radial breathing mode of DWCNTs grown from $FeCp_2$@SWCNTs for excitation with different lasers as indicated. The spectrum at the bottom compares the results with the response from unfilled tubes excited with 457 nm radiation. Asterisks assign intermediate frequency contributions from the outer tubes.

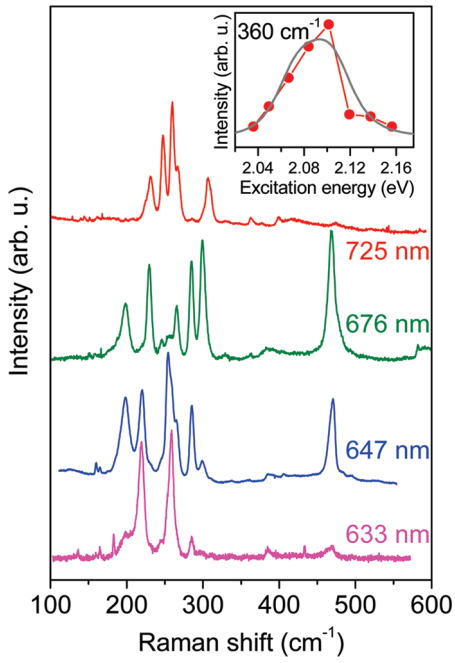

Figure 5. Resonance excitation of the RBM line at 470 cm^{-1}. The inset depicts the cross section for the line at 360 cm^{-1} (see Figure 4, 600 nm spectrum). The solid line is as calculated.

frequency range show up instead. An example is given in Figure 3, which depicts spectra before and after transformation to DWCNTs. To observe the new lines, a wide set of laser excitations is needed, as they originate from the RBMs of the small diameter tubes which have characteristic resonance transitions. Figure 4 depicts a set of Raman spectra excited with lasers from deep blue to deep red (for details, see Supporting Information). As indicated, each laser reveals characteristic vibrational modes. Interestingly, the lines exhibit some structure but not the strongly expressed grouping as it has been observed for DWCNTs with conventional sized outer tubes.[21] Also, the line widths are broader and usually exhibit an asymmetric shape compared to conventionally grown DWCNTs. The larger line widths can be due to a length distribution of inner tube segments as they were observed in the HRTEM analyses (see below). The strongest line observed from the inner tubes appears at 470 cm^{-1} for excitation with a 676 nm laser. The line intensity is higher than the intensities from the outer tubes even though much less carbon material is involved due to smaller tube size and incomplete filling. This means that the laser used is close to resonance, and the scattering cross section is strongly enhanced due to enhanced electron−phonon coupling.

The resonance behavior of the 470 cm^{-1} line can be well studied by using different lasers in the red spectral region. Results are depicted in Figure 5. The left part of the figure shows the resonance behavior of the outer tube RBM lines with an average resonance width of 120 meV for each peak (for details, see Supporting Information). Cross section measurements work even better for the Raman line at 360 cm^{-1}, where the continuously tunable dye laser can be used. A result is depicted in the insert of the figure. The solid line is calculated according to the theory of Martin and Falicov.[22]

$$I(E_L) \propto \frac{1}{|(E_L - E_{ii} - i\Gamma)(E_L - E_{RBM} - E_{ii} - i\Gamma)|^2} \quad (1)$$

where E_L, E_{RBM}, and Γ are the laser energy, the energy of the RBM, and the line width parameter, respectively. For convenience, the same value of 0.025 eV for Γ is used for the incoming and outgoing resonance. The two resonances appear at different positions but are strongly overlapping. E_{ii} is the transition energy defined in eq 2. The narrow resonance width of only 45 meV is typical for the observed lines. It allows one to obtain information on the resonance position for any observed Raman line even if the cross section could not be measured explicitly. The resonance width is only slightly

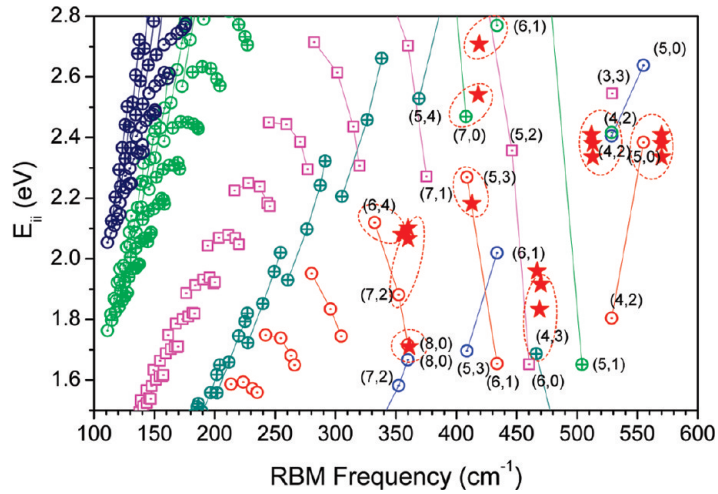

Figure 6. Transition energy−wavenumber diagram (Kataura−Popov plot) for narrow diameter tubes. The symbols are as calculated from eq 2. Lines connect the calculated data for the same family. Different symbols are used for type I (open circles), type II (circles with cross), and for metallic tubes (open squares). Asterisks (red) represent experimental data.

TABLE 1. Experimental Results for RBM Frequencies (Column 1) and Corresponding Laser Excitation Energies (Column 2) with the Assignment (Column 3) Compared to Calculated Values for the Frequencies and Transition Energies from Equation 2 (Columns 4 and 5). Last Column Has the Transition Energies from the DFT Calculations Using the Siesta Package[28]

experiment			calculated		DFT
ν (cm^{-1})	laser (eV)	assignment (n,m)	ν (cm^{-1})	E_{ii} (eV)	E_{ii} (eV)
570	2.38	(5,0)	555	2.38 (E_{22})	2.4
513	2.38	(4,2)	529	2.40 (E_{11})	2.5
470	1.83	(4,3)	466	1.69 (E_{11})	1.73
419	2.71	(6,1)	434	2.77 (E_{33})	
417	2.54	(7,0)	408	2.47 (E_{33})	2.7
413	2.18	(5,3)	409	2.27 (E_{22})	
363	1.71	(8,0)	360	1.72 (E_{22})	1.7
360	2.06	(7,2)	352	1.88 (E_{22})	
355	2.08	(6,4)	332	2.12 (E_{22})	

broader than the 30 meV widths for the cross sections of inner tubes in conventionally sized DWCNTs.[23]

The good definition of the resonance transition energies allows one to plot them together with the RBM frequencies on a Kataura plot especially derived for the ultrahigh curvature tubes. This plot was generated from the bare results of Popov[24] by correcting them according to the theoretical model of Kane and Mele.[25] The procedure used was similar to the work of Jorio *et al.*,[26] except that the starting point was from the symmetry adapted non-orthogonal tight-binding model of Popov. Thus, the transition energies were calculated from

$$E_{jj}(p, d_{DFT}, \theta) = E_{p,jj} + \frac{a'p}{d_{DFT}}\left[\log_{10}\frac{c}{p/d_{DFT}}\right] + \frac{\beta_p \cos(3\theta)}{d_{DFT}^2} \quad (2)$$

where $E_{p,jj}$ are the values for the transition energies obtained by Popov *et al.*, $a' = 0.16$ and $c = 5.25$ are empirical constants; $p = 1-4$ are the transition numbers for E_{11}^S, E_{22}^S, E_{11}^M, and E_{33}^S, respectively; θ is the chiral angle, and β_p are family selective parameters with a value of 0.046 for E_{22}^S transitions in semiconducting type 2 tubes (see Supporting Information). The DFT diameter was obtained from[27] $1/d_{DFT} = 1/d(n,m) - 0.005/d(n,m)^2 + 0.0013/d(n,m)^4$, where $d(n,m)$ is the tight-binding tube diameter. Equation 2 has a logarithmic correction term which takes care of many electron effects. The empirical parameters were set to match the results for HiPco material. Equation 2 may be extrapolated to even smaller tubes and can thus be used to represent the present data. They match very well to transition energies evaluated from the DFT calculations. Figure 6 depicts the transition energy *versus* frequency relations from eq 2 and values for the RBM corrected for chirality effects,[26] again using the d_{DFT} for the tube diameter (for details, see Supporting Information). The symbols are explained in the figure caption. As can be seen, there is a dramatic family spread of more than 2 eV, for example, for family 12, which results in a very strong deviation of the transition energies from the $1/d_t$ law known for standard diameter tubes. For example, the E_{11}^M energy for the (6,0) tube comes down from 5.3 to 1.63 eV. In addition, a cross over between transitions energies is already obtained for the E_{11} and E_{22} transitions. This is, for example, seen for the (6,1) tube where E_{22} (1.63 eV) has a lower energy than E_{11} (2 eV).

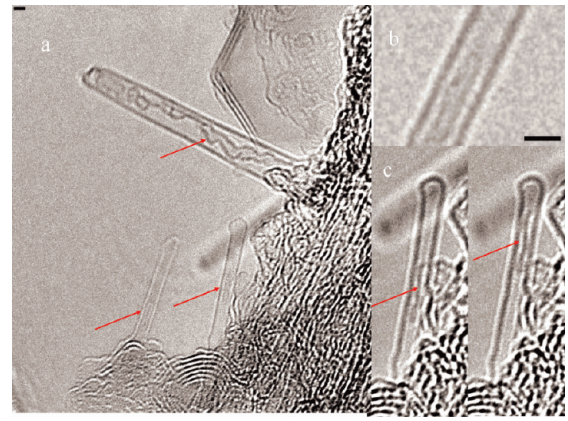

Figure 7. Transmission electron micrographs of DWCNTs grown from $FeCp_2$ peapods. (a) Enlarged area with three tubes resolved. Two of them contain a section of an inner tube inside a longer outer tube (red arrows). Due to different focus, one of the two inner tubes is visible as white contrast, while the other one is visible as dark contrast. The third feature in focus depicts a tube with carbon filling without forming an inner tube. (b) High-resolution imaging demonstrating that inner tubes are capped. Scale bar = 1 nm in both pictures. (c) Two consecutive recordings of the same tube. It demonstrates the mobility of the inner tube segments (arrows) in the electron beam.

The experimental observations were inserted into Figure 6 and allow for a tentative assignment of the observed RBMs to tube chiralities as indicated by the dashed circles. This assignment is summarized for all observed tubes in Table 1 together with calculated values from eq 2 as well as with calculations from the Siesta package[28] (for details, see Supporting Information). The averaged deviation between observed and calculated frequencies is $+4$ cm^{-1}, which is assigned to an upshift of the RBM frequency due to tube−tube interaction. This value is slightly smaller than the average value observed for the upshift of inner tube RBM frequencies from conventionally sized DWCNTs. The discrepancy is probably due to the observation of a large number of satellite lines in the latter case where inner tubes grow also in rather narrow outer tubes.

After subtraction of the 4 wave numbers the root-mean-square error between experiment and calculation is ± 4.2 cm^{-1} or about 1%. Similarly, the mean deviation for the transition energies is 0.019 eV with a root-mean-square error of ± 0.08 eV or 4%. The results from the DFT calculations match very well to the results of eq 2 and thus confirm its applicability.

A final check on the nature and size of the DWCNTs grown from $FeCp_2$ peapods was done by high-

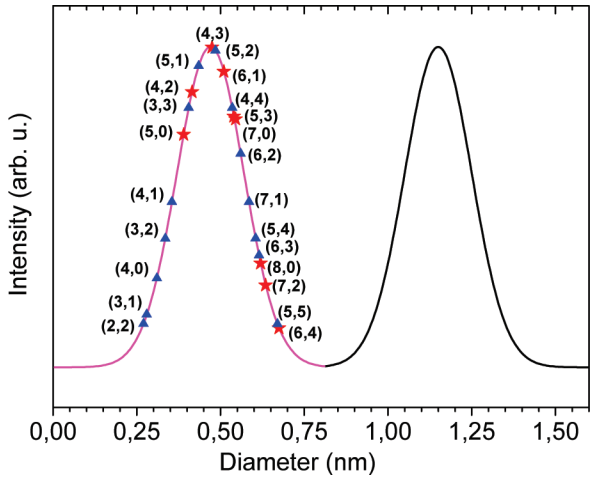

Figure 8. Diameter distribution for DWCNTs. For the inner tubes, the discrete (*n*,*m*) values are explicitly indicated: (red) asterisks, observed; (blue) triangles, not observed.

resolution TEM. Figure 7 has some selected results. Part a shows a selected large-scale area with several filled tubes. Two of them exhibit segments of inner tubes. For the outer tubes, in some cases, length calibration could be performed from the Fourier analysis of the tube pattern. For the tube on the right side, this revealed a tube diameter of 1.08 nm corresponding to a (12,3) tube. The inner tube diameter was read from the image to be 0.4 ± 0.02 nm. The corresponding diameter difference is slightly larger than the values known from the growth of DWCNTs from fullerene peapods but consistent with experiences for the catalytic growth of DWCNTs from ferrocene.[17] The third feature in part a with a diameter of 1.8 nm has some carbon filling, but no inner tube was formed. Part b is a high-resolution image demonstrating capping of the inner tubes. The two pictures in part c are snapshots of an animation that demonstrates the motion of inner tubes in a partially filled outer tube (see Supporting Information). Due to defocusing during the imaging, the inner tubes appear as lines. Images taken at different defocus confirm that the observed feature is indeed a nanotube segment. Evidently, the segment of the inner tube is mobile in the electron beam. The video in Supporting Information shows the translation of this inner tube under the beam.

The presented results demonstrate that DWCNTs grown from ferrocene in small diameter host tubes are an excellent source to investigate ultrahigh curvature tubes. With ferrocene as a filler, almost the limit for stability toward small diameters is reached. Figure 8 shows the diameter distribution, fitted as a Gaussian to experimental values from optical absorption for the outer tubes, and the 0.66 nm downshifted distribution for the inner tubes as a full line. For the inner tubes, the individual tube species are marked. The graph immediately explains why the (4,3) tube has the strongest Raman signal. It belongs to one of the most abundant species and is obviously excited in good resonance at 676 nm excitation, as shown in Figure 5. All tubes inserted with a (blue) triangle are either at the lower edge of the diameter distribution or exhibit transition energies which are out of the visible spectral range. No tubes with (tight-binding) diameters below 0.39 nm could be observed. The (3,3) tube is metallic with a resonance close to 3 eV, which is at the edge of the available set of laser lines. Tube (5,1) has resonances at 1.65 and 3.8 eV. Tubes with curvature higher than (5,0) probably did not grow due to high curvature energy.

Calculations including correction terms according to eq 2 and the results from DFT are in very good agreement with experiment. The small discrepancies are not surprising since the experiments were carried out for a tube@tube geometry, whereas the calculations were performed for free tubes. For the DFT calculations, dielectric shielding is another source for small deviations. Also, the cancellation between correlations increasing the energy scale and excitons reducing the scale is certainly not perfect. Deviation between experiment and calculations must be seen relative to the overall change of several electronvolts induced by the high curvature.

The derivation of the transition energies from eq 2 still uses family behavior. However, since the sequence on an energy scale is not at all unidirectional, assignment as transitions corresponding to families is not meaningful any more. Rather, transition energy enumeration should be used as it is derived from the *ab initio* calculations.

The calculations on the filling and the TEM results show that only a partial filling of the host tube is possible. However, since the inner tube fragments are mobile, additional filling of the already prepared DWCNTs should be possible.

CONCLUSION

The inner shell tubes of DWCNTs grown from HiPco tubes with a mean diameter of only 1.1 nm are shown to be good examples for SWCNTs with ultrahigh curvature. The narrow diameter inner tubes were obtained using ferrocene inside the tubes as a carbon source. From molecular dynamical calculations, tubes with chiral indices as low as (12,0) exhibit already a bound state with the ferrocene which, on transformation to DWCNTs, could provide a (3,0) or (2,2) tube. In the experiments, the smallest observed inner tube had the chiral indices of (5,0). This corresponds to a DFT diameter of 0.406 nm (tight-binding diameter 0.391 nm). Resonance Raman scattering, TEM, and calculations on various levels revealed information on the geometrical, vibrational, and electronic structure. All tubes in the diameter range between 0.406 and 0.66 nm, which have resonance transition in the visible spectral range, could be observed, except the near armchair (5,4) species. Dramatic deviations of several electronvolts for the transition energies were obtained from the calcula-

tions compared to results for a tight-binding model, resulting in a family spread of more than 2 eV. The deviations were found to be in very good agreement with the transition energies determined from the resonance Raman experiments. The TEM experiments confirmed the partial filling of the HiPco material with very narrow diameter tubes and revealed a noticeable mobility of the inner tube fragments in the electron beam.

MATERIALS AND METHODS

HiPco tubes were purchased from Tubes at Rice. The diameter distribution was determined by optical absorption and resonance Raman, where corrections according to eq 2 were considered.[29] Assuming a Gaussian distribution, the resulting mean diameter was 1.1 ± 0.05 nm with a fwhm of 0.25 nm. The tubes were opened by exposure to air at 420 °C for 1 h and subsequently filled by heating for 48 h at nominal 400 °C in $FeCp_2$ vapor in a sealed quartz tube. For the transformation to DWCNTs, the resulting peapods were again vacuum sealed into a quartz tube and exposed for 1 h to 800 °C. To remove non-encapsulated ferrocene, the peapod material was annealed in dynamic vacuum at 400 °C for 2 h. From the low transformation temperature, it is concluded that the inner tubes grow catalytically with Fe_3C (iron carbide) as the catalytic particle. As it was demonstrated previously, the catalytic particle stays inside the tubes unless it is released by high-temperature vacuum annealing.[17]

Raman analysis for samples in the form of bucky paper was performed at all intermediate steps with a Dilor *xy* triple monochromator system with a broad spectrum of laser lines, including tunable systems. For cross section measurements, the Raman response was calibrated using results from Si[30] (see Supporting Information).

For the TEM analysis, an image side aberration corrected FEI Titan 80-300 microscope was used, at 80 keV to avoid electron beam damage. Diameter determination follows the analysis of ref 31 to take into account the differences in apparent and actual tube diameter.

To describe the structure and energetics of the peapods, we employed Brenner potential for nanotubes and MM3 potential for ferrocene and NT−$FeCp_2$ interactions, a well tested protocol implemented by us in Tinker.[32] Geometries and binding energies of minima were obtained from quenched molecular dynamics (QMD) simulations (for details, see Supporting Information). To evaluate the electronic structure, we used the basic results from Popov *et al.*,[24] which were corrected for many electron contributions and chirality effects according to Kane and Mele[25] and Jorio *et al.*[26] The results were compared to DFT calculations from the Siesta package[28] using double-ζ accuracy for the atomic orbital basis set (see Supporting Information).

Acknowledgment. Work supported by the Fonds zur Förderung der Wissenschaftlichen Forschung (FWF) Project I83-N20 (ESF IMPRESS) and by the Deutsche Forschungsgemeinschaft (DFG), Project PI 440/3-2. Valuable discussions with Prof. Th. Pichler (U Wien, A), L. Wirtz (U Lille, F), and E. Molinari (IdN CNR Modena, I) are greatly acknowledged.

Supporting Information Available: Experimental procedures, details on calculational methods for ferrocene peapods and DWCNTs. Movie showing the mobility of an inner tube fragment in the TEM electron beam. This material is available free of charge *via* the Internet at http://pubs.acs.org.

REFERENCES AND NOTES

1. Saito, R.; Dresselhaus, G.; Dresselhaus, M. *Physical Properties of Carbon Nanotubes*; Imperial College Press: London, 1998.
2. Dresselhaus, M. S.; Dresselhaus, G.; Avouris, P. *Carbon Nanotubes: Synthesis, Structure, Properties, and Applications*; Springer: Berlin, 2001.
3. Reich, S.; Thomsen, C.; Maultzsch, J. *Carbon Nanotubes*; Wiley-VCH: Weinheim, Germany, 2004.
4. Kürti, J.; Zólyomi, V.; Kertesz, M.; Guangyu, S. The Geometry and the Radial Breathing Mode of Carbon Nanotubes: Beyond the Ideal Behaviour. *New J. Phys.* **2003**, *5*, 125.
5. Spataru, C. D.; Ismail-Beigi, S.; Benedict, L. X.; Louie, S. G. Excitonic Effects and Optical Spectra of Single-Walled Carbon Nanotubes. *Phys. Rev. Lett.* **2004**, *92*, 077402-1-4.
6. Chang, E.; Bussi, G.; Ruini, A.; Molinari, E. First-Principles Approach for the Calculation of Optical Properties of One-Dimensional Systems with Helical Symmetry: The Case of Carbon Nanotubes. *Phys. Rev. B* **2005**, *72*, 195423.
7. Okada, S.; Oshiyama, A. Curvature-Induced Metallization of Double-Walled Semiconducting Zigzag Carbon Nanotubes. *Phys. Rev. Lett.* **2003**, *91*, 216801-1–216801-4.
8. Zólyomi, V.; Koltai, J.; Rusznyák, A.; Kürti, J.; Gali, A.; Simon, F.; Kuzmany, H.; Szabados, A.; Surján, P. R. Intershell Interaction in Double Walled Carbon Nanotubes: Charge Transfer and Orbital Mixing. *Phys. Rev. B* **2008**, *77*, 245403-1–245403-10.
9. Bohnen, K. P.; Heid, R.; Liu, H. J.; Chan, C. T. Lattice Dynamics and Electron−Phonon Interaction in (3,3) Carbon Nanotubes. *Phys. Rev. Lett.* **2004**, *93*, 245501-1–245501-4.
10. Benedict, L. X.; Crespi, V. H.; Louie, S. G.; Cohen, M. L. Static Conductivity and Superconductivity of Carbon Nanotubes: Relations between Tubes and Sheets. *Phys. Rev. B* **1995**, *52*, 14935–14940.
11. Connétable, D.; Rignanese, G.-M.; Charlier, J.-C.; Blase, X. Room Temperature Peierls Distortion in Small Diameter Nanotubes. *Phys. Rev. Lett.* **2005**, *94*, 015503-1-4.
12. Kuemmeth, F.; Ilani, S.; Ralph, D. C.; McEuen, P. L. Coupling of Spin and Orbital Motion of Electrons in Carbon Nanotubes. *Nature* **2008**, *452*, 448–452.
13. Lortza, R.; Zhang, Q.; Shi, W.; Ye, J. T.; Qiu, C.; Wang, Z.; He, H.; Sheng, P.; Qian, T.; Tang, Z.; *et al.* Superconducting Characteristics of 4-Angstrom Carbon Nanotube-Zeolite Composite. *Proc. Natl. Acad. Sci. U.S.A.* **2009**, *106*, 7299–7303.
14. Tang, Z. K.; Zhai, J. P.; Tong, Y. Y.; Hu, X. J.; Saito, R.; Feng, Y. J.; Sheng, P. Resonant Raman Scattering of the Smallest Single-Walled Carbon Nanotubes. *Phys. Rev. Lett.* **2008**, *101*, 047402.
15. Bandow, S.; Takizawa, M.; Hirahara, K.; Yudasaka, M.; Iijima, S. Raman Scattering Study of Double-Wall Carbon Nanotubes Derived from the Chains of Fullerenes in Single-Wall Carbon Nanotubes. *Chem. Phys. Lett.* **2001**, *337*, 48–54.
16. Pfeiffer, R.; Holzweber, M.; Peterlik, H.; Kuzmany, H.; Liu, Z.; Suenaga, K.; Kataura, H. Dynamics of Carbon Nanotube Growth from Fullerenes. *Nano Lett.* **2008**, *7*, 2428–2434.
17. Shiozawa, H.; Pichler, T.; Grueneis, A.; Pfeiffer, R.; Kuzmany, H.; Liu, Z.; Suenaga, K.; Kataura, H. A Catalytic Reaction Inside a Single-Walled Carbon Nanotube. *Adv. Mater.* **2008**, *20*, 1443.
18. Shiozawa, H.; Kramberger, C.; Pfeiffer, R.; Kuzmany, H.; Pichler, T.; Liu, Z.; Suenaga, K.; Kataura, H.; Silva, S. R. P. Catalyst and Chirality Dependent Growth of Carbon Nanotubes Determined through Nano Test Tube Chemistry. *Adv. Mater.* DOI 10.1002/adma.201001211 (2010).
19. Guan, L.; Suenaga, K.; Iijima, S. Smallest Carbon Nanotube Assigned with Atomic Resolution Accuracy. *Nano Lett.* **2008**, *8*, 459–462.
20. Li, L.; Khlobystov, A.; Wiltshire, J.; Briggs, G.; Nicholas, R. Diameter-Selective Encapsulation of Metallocenes in Single-Walled Carbon Nanotubes. *Nat. Mater.* **2005**, *4*, 481–485.
21. Pfeiffer, R.; Kuzmany, H.; Simon, F.; Bokova, S. N.;

Obraztsova, E. Resonance Raman Scattering from Phonon Overtones in Double-Wall Carbon Nanotubes. *Phys. Rev. B* **2005**, *71*, 155409-1–155409-8.
22. Martin, R. M.; Falicov, L. M. In *Resonance Raman Scattering*; Springer: Berlin, 1983; p 79.
23. Simon, F.; Pfeiffer, R.; Kuzmany, H. Temperature Dependence of the Optical Excitation Lifetime and Band Gap in Chirality Assigned Semiconducting Single-Wall Carbon Nanotubes. *Phys. Rev. B* **2006**, *74*, 121411(R).
24. Popov, V. N. Curvature Effects on the Structural, Electronic and Optical Properties of Isolated Single-Walled Carbon Nanotubes within a Symmetry-Adapted Non-orthogonal Tight-Binding Model. *New J. Phys.* **2004**, *6*, 17.
25. Kane, C. L.; Mele, E. J. Electron Interactions and Scaling Relations for Optical Excitations in Carbon Nanotubes. *Phys. Rev. Lett.* **2004**, *93*, 197402.
26. Jorio, A.; Fantini, C.; Pimenta, M. A.; Capaz, R. B.; Samsonidze, G. G.; Dresselhaus, G.; Dresselhaus, M. S.; Jiang, J.; Kobayashi, N.; Grüneis, A.; *et al.* Resonance Raman Spectroscopy (*n,m*)-Dependent Effects in Small-Diameter Single-Wall Carbon Nanotubes. *Phys. Rev. B* **2005**, *71*, 075401.
27. Kramberger, C.; Pfeiffer, R.; Kuzmany, H.; Zólyomi, V.; Kürti, J. Assignment of Chiral Vectors in Carbon Nanotubes. *Phys. Rev. B* **2003**, *68*, 235404.
28. Soler, J.; Artacho, E.; Gale, J.; Garcia, A.; Junquera, J.; Ordejon, P.; Sanchez-Portal, D. The SIESTA Method for *Ab Initio* Order-N Materials Simulation. *J. Phys.:Condens. Mater* **2002**, *14*, 2745–2779.
29. Kuzmany, H.; Plank, W.; Peterlik, H. Unpublished results.
30. Renucci, J. B.; Tyte, R. N.; Cardona, M. Resonant Raman Scattering in Silicon. *Phys. Rev. B* **1975**, *11*, 3885–3895.
31. Qin, C.; Peng, L. Measurement Accuracy of the Diameter of a Carbon Nanotube from TEM Images. *Phys. Rev. B* **2002**, *65*, 155431.
32. Melle-Franco, M.; Kuzmany, H.; Zerbetto, F. Mechanical Interaction in All-Carbon Peapods. *J. Phys. Chem. B* **2003**, *109*, 6986–6990.